Numerical studies of the interaction of an atomic sample with the electromagnetic field in two dimensions

Maxim Sukharev[1,*] and Abraham Nitzan[2,†]

[1]*Department of Applied Sciences and Mathematics, Arizona State University, Mesa, Arizona 85212, USA*
[2]*School of Chemistry, Tel Aviv University, Tel Aviv IL-69978, Israel*

We consider the interaction of electromagnetic radiation of arbitrary polarization with multilevel atoms in a self-consistent manner, taking into account both spatial and temporal dependencies of local fields. This is done by numerically solving the corresponding system of coupled Maxwell-Liouville equations for various geometries. In particular, we scrutinize linear optical properties of nanoscale atomic clusters, demonstrating the significant role played by collective effects and dephasing. It is shown that subwavelength atomic clusters exhibit two resonant modes, one of which is localized slightly below the atomic transition frequency of an individual atom, while the other is positioned considerably above it. As an initial exploration of future applications of this approach, the optical response of core-shell nanostructures, with a core consisting of silver and a shell composed of resonant atoms, is examined.

PACS number(s): 42.50.Ct, 78.67.−n

I. INTRODUCTION

Nanoscale optical materials have long been attracting considerable attention due to many important applications ranging from optical nanodevices [1], plasmonic circuitry [2], nanoscale sources of coherent radiation [3], single atom or molecule manipulation [4], biomedical applications [5,6], and many others. Among such exciting applications lies the yet-to-be explored subfield of nanoscale optical atomic and molecular physics that deals with ensembles of atoms or molecules interacting with dielectric nanoparticles (NP) and their assemblies. Such systems are characterized by a significant spatial dependence of evanescent electromagnetic (EM) fields on the dielectric environment, providing the means to control the behavior of molecular systems by the combination of large EM fields and large field gradients, exemplified by recent work [7–12] on the EM field associated with metal NP dimers and their dependence on particle size and interparticle distance. At their core, these phenomena rely mostly on the excitations of surface plasmon-polariton (SPP) resonances [13] in systems comprising metal NPs and their arrays [14], as well as other nanoscale metal surfaces, such as subwavelength diffraction gratings, whose optical properties depend sensitively on their surface topology and material parameters [15]. Their studies have lead to many applications such as coherent EM energy transport in space [16], surface-enhanced Raman spectroscopy (SERS) [17] and tip-enhanced microscopy [18]. Recent attention has focused on optical control scenarios, ranging from coupled exciton-plasmon dynamics in semiconductor nanodots [19–27] and in molecular aggregates [28–36], where metal NPs affect excitation energy transfer between molecules, to optical trapping of single atoms or molecules [37–40]. Such applications are facilitated by the possibility to control the geometry of nanomaterials (NP size, their relative arrangement, etc.) with an outstanding precision [41].

While theoretical and computational methodologies for studying these phenomena have advanced considerably, the consequences of mutual feedback between molecular excitations and metallic SPP resonances are not well understood, especially when one probes systems comprising both metallic nanostructures and semiconductor or molecular particles or layers. A simple and often-used description is based on assigning a dielectric response function to the semiconductor or molecular component and solving the electromagnetic problem for the corresponding composite dielectric. While such an approach can be useful for describing the effect of the molecular environment on the metallic plasmon, it cannot be used to describe energy-transfer, relaxation, and spontaneous emission in the excitonic (molecular or semiconductor) system. It is hence important to develop a self-consistent description of the electromagnetic response of such systems. Such an approach has to take into account the electrodynamics of the radiation field and the quantum dynamics of the molecular system in a self-consistent manner. This can be accomplished by solving simultaneously Maxwell's equations for the radiation field and the Liouville equation for the molecular density matrix, including the molecular polarization current in the former and the molecule-field interaction in the latter.

First attempts to consider numerically coupled Maxwell-Bloch equations have been initiated by Ziolkowski *et al.* [42,43] for simple two-level atoms in one and two dimensions utilizing a finite-difference time-domain (FDTD) technique. Later on, this approach has been extended to three dimensions [44]. Although these works contain interesting and important physics, they are limited to ensembles of two-level systems. Consideration of multilevel systems is critical for modeling of nanolasing, which has to include at least three levels. Moreover, the proposed numerical implementation results in noticeably long execution times. The scheme we propose is more efficient, as discussed below. Similarly, Neuhauser *et al.* proposed another approach [45] where the authors coupled Maxwell's equations to the Schrödinger equation describing a molecule located in the closed proximity of a metal NP.

*maxim.sukharev@asu.edu
†nitzan@post.tau.ac.il

These works, however, cannot in their present form include relaxation and dephasing effects, which, as we demonstrate, are very important.

In this paper we describe a numerical implementation of such a model, using the methodology developed by Ziolkowski *et al.* [42,43] as our starting point. This model captures collective effects that play a pivotal role in electrodynamics of nanosystems, as well as the counterbalancing effect of dephasing processes. The questions to be addressed are

(1) How does a size of the system affect scattering and absorption of EM radiation?

(2) What is a role of dephasing and relaxation effects?

(3) When does one observe a collective response of atoms to external EM excitation?

These and other closely related questions are not only important from the fundamental point of view (how optically induced interatomic or intermolecular interactions depend on structural and material parameters), but are also essential for a general understanding of the optics of many-body systems.

In this regard it should be pointed out that, although the technique we propose in this paper is utilized to capture collective effects of quantum particles in the linear response regime, it can easily be applied to nonlinear systems.

The paper is organized as follows: Section II discusses our computational approach, based on coupled Maxwell-Liouville equations in the mean-field approximation. In Sec. III we provide details of the numerical implementation. Section IV describes and discusses the results of our numerical studies. Our main conclusions along with the future research outlook are presented in Sec. V.

II. MODEL

We consider a general problem of a system of quantum particles (further referred to as atoms) interacting with EM radiation. We start from the time-domain Maxwell's equations for the dynamics of the EM fields, $\vec{E}$ and $\vec{H}$:

$$\mu_0 \frac{\partial \vec{H}}{\partial t} = -\nabla \times \vec{E}, \tag{1a}$$

$$\varepsilon_0 \frac{\partial \vec{E}}{\partial t} = \nabla \times \vec{H} - \vec{J}, \tag{1b}$$

where μ_0 and ε_0 are the magnetic permeability and dielectric permittivity of free space, respectively. In spatial regions occupied by a metal nanostructure (such as a metal NP, for instance) Eq. (1b) is evaluated in the standard way from the metal dielectric dispersion [46]. In the present study, the dispersion of the dielectric constant of metal, $\varepsilon(\omega)$, is taken in the form of the Drude model

$$\varepsilon(\omega) = \varepsilon_r - \frac{\omega_p^2}{\omega^2 - i\gamma\omega}, \tag{2}$$

with numerical parameters describing silver for the wavelengths of interest: $\varepsilon_r = 8.26$, $\omega_p = 1.76 \times 10^{16}$ rad/s, $\gamma = 3.08 \times 10^{14}$ rad/s. The time evolution of the current density $\vec{J}$ in metal regions is then

$$\frac{\partial \vec{J}}{\partial t} = a\vec{J} + b\vec{E}, \tag{3}$$

where $a = -\gamma$ and $b = \varepsilon_0 \omega_p^2$.

In the spatial regions occupied by atoms, the mutual interaction between the atomic system and the EM field is accounted for in a self-consistent manner as follows: First, the current density in Eq. (1b) is expressed in terms of the macroscopic polarization of the atomic system, $\vec{P}(\vec{r},t)$:

$$\vec{J} = \frac{\partial \vec{P}}{\partial t}. \tag{4}$$

The latter is given by

$$\vec{P} = n_a \langle \vec{\mu} \rangle, \tag{5}$$

where

$$\langle \vec{\mu} \rangle = \text{Tr}(\hat{\rho}\vec{\mu}) \tag{6}$$

is the expectation value of the atomic dipole moment and n_a is the atomic density. Equations (4)–(6) constitute the main approximation of the present approach, whereupon the local polarizability is expressed in terms of the local atomic density multiplied by the local averaged single atomic dipole. The time evolution of the latter is obtained from the evolution of the single-atom density matrix (described below) in the presence of the EM field, thus providing a self-consistent description of the field-matter dynamics.

Next, consider the atomic subsystem. While our ultimate goal is to study realistic three-dimensional systems, the present study focuses on nanoscale atomic clusters in two dimensions, which are taken to lie in the XY plane [47]. The incident radiation field is represented by a transverse-electric (TE) mode with respect to z axis. It is characterized by two in-plane electric field components, E_x and E_y, and one out-of-plane magnetic field component, H_z. To account for the (two-dimensional) spherical symmetry of the atomic polarization response, the atoms are described as three-level systems: an s-type ground state and two degenerate p-type excited states of p_x and p_y character [as depicted in Fig. 1(a)]. In anticipation of possible generalizations to more complex models involving multilevel systems we use, in what follows, a basis of angular momentum wave functions with quantization axis in the z direction, $|1\rangle = |s\rangle$, $|2\rangle = (|p_x\rangle + i|p_y\rangle)/\sqrt{2}$, $|3\rangle = (|p_x\rangle - i|p_y\rangle)/\sqrt{2}$, with optical transitions corresponding to $\Delta J = \pm 1$ and $\Delta M = \pm 1$ selection rules. The corresponding Hamiltonian is

$$\hat{H} = \hat{H}_0 - \vec{\mu} \cdot \vec{E}(t) = \begin{pmatrix} 0 & \Omega_-(t) & -\Omega_+(t) \\ \Omega_+(t) & \hbar\omega_a & 0 \\ -\Omega_-(t) & 0 & \hbar\omega_a \end{pmatrix}, \tag{7}$$

where $\hbar\omega_a$ is the atomic energy transition, $\Omega_\pm = \mu_{sp}[E_x(t) \pm iE_y(t)]/\sqrt{6}$, and μ_{sp} is the s-p matrix element of the dipole moment operator, that, in principle, can be taken from experiment or calculated using standard quantum chemistry packages. The Cartesian components of the dipole moment operator are

$$\hat{\mu}_x = -\frac{\partial \hat{H}}{\partial E_x} = \frac{\mu_{sp}}{\sqrt{6}} \begin{pmatrix} 0 & -1 & 1 \\ -1 & 0 & 0 \\ 1 & 0 & 0 \end{pmatrix}, \tag{8a}$$

$$\hat{\mu}_y = -\frac{\partial \hat{H}}{\partial E_y} = \frac{\mu_{sp}}{\sqrt{6}} \begin{pmatrix} 0 & i & i \\ -i & 0 & 0 \\ -i & 0 & 0 \end{pmatrix}. \tag{8b}$$
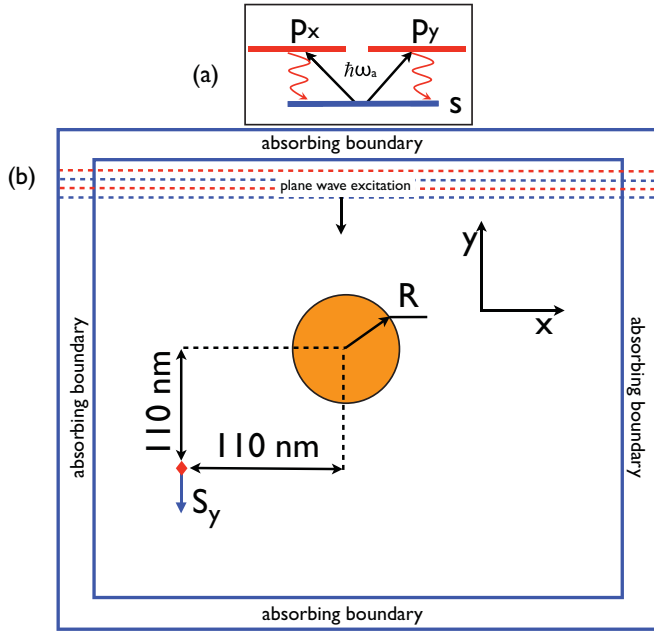
FIG. 1. (Color online) Panel (a) shows the energy level diagram of a two-level two-dimensional atom with black arrows indicating optically induced transitions by the TE mode and red arrows representing spontaneous decay. Panel (b) depicts schematics of the simulations with the detection point shown as a red diamond (in the lower-left corner), where the y component of the Poynting vector is calculated.

Note that the dipole moment operator (8) differs from the one used in [43] by the factor of $\sqrt{3}$.

The mean-field approximation Eq. (5) makes it possible to describe the atomic system in terms of the single-atom density matrix $\hat{\rho}$, which satisfies the Liouville equation

$$i\hbar \frac{d\hat{\rho}}{dt} = [\hat{H}, \hat{\rho}] - i\hbar\hat{\Gamma}\hat{\rho}. \tag{9}$$

Equation (9) describes the time evolution of an atom interacting with the radiation field and subject to (assumed Markovian) relaxation processes described by the $\hat{\Gamma}$ operator, which is taken in the Lindblad form [48]. The diagonal elements of this operator correspond to excited-state lifetimes, while nondiagonal elements account for dephasing effects.

Equations (1)–(9) describe the time evolution of the atomic system and radiation field in a self-consistent way. Note that, in the single-atom Hamiltonian $\hat{H}$ given by Eq. (7), interatomic interactions are absent. Still, the dynamics described by Eqs. (1)–(9) is not that of independent atoms: the self-consistent scheme accounts for all interactions between atoms that are associated with their mutual interaction with the radiation field, including excitonic (energy-transfer) interactions, which are all important for elucidating the overall system response. Note that, assuming that the EM field does not significantly vary within a volume occupied by a single atom, the spatial dependence of the density matrix in Eq. (9) depends parametrically on position via the EM field variables.

Equations (8) and (9) lead to the following equations for the atomic density matrix elements:

$$\frac{d\rho_{11}}{dt} = i\omega_+(\rho_{12} + \rho_{13}^*) - i\omega_-(\rho_{13} + \rho_{12}^*) + \gamma_1(\rho_{22} + \rho_{33}), \tag{10a}$$

$$\frac{d\rho_{12}}{dt} = i\omega_a\rho_{12} - i\omega_-(\rho_{22} - \rho_{11}) + i\omega_+\rho_{23}^* - \gamma_2\rho_{12}, \tag{10b}$$

$$\frac{d\rho_{13}}{dt} = i\omega_a\rho_{13} + i\omega_+(\rho_{33} - \rho_{11}) - i\omega_-\rho_{23} - \gamma_2\rho_{13}, \tag{10c}$$

$$\frac{d\rho_{22}}{dt} = i\omega_-\rho_{12}^* - i\omega_+\rho_{12} - \gamma_1\rho_{22}, \tag{10d}$$

$$\frac{d\rho_{23}}{dt} = -i\omega_+(\rho_{13} + \rho_{12}^*) - 2\gamma_2\rho_{23}, \tag{10e}$$

$$\frac{d\rho_{33}}{dt} = i\omega_-\rho_{13} - i\omega_+\rho_{13}^* - \gamma_1\rho_{33}, \tag{10f}$$

where $\omega_\pm = \Omega_\pm/\hbar$ and $\gamma_2 = \gamma_p + \gamma_1/2$ with γ_p denoting the pure dephasing rate due to environmentally induced random fluctuations in the atomic energy spacing. As noted above, in Eq. (10) we denoted the ground state as $|1\rangle$ and the excited states $|J = 1, M = -1\rangle$ and $|J = 1, M = 1\rangle$ as $|2\rangle$ and $|3\rangle$, respectively.

Finally, by using Eqs. (8) and (10) we obtain the macroscopic polarization current [time derivative of Eq. (5)], which enters Ampère's law (1b)

$$\frac{\partial \vec{P}}{\partial t} = n_a \frac{\partial \langle \vec{\mu} \rangle}{\partial t}, \tag{11a}$$

where, back in Cartesian coordinates,

$$\frac{\partial \langle \mu_x \rangle}{\partial t} = \frac{E_y \mu_{sp}^2}{3\hbar}(\rho_{22} - \rho_{33}) - i\frac{\mu_{sp}}{\sqrt{6}}[(\omega_a + i\gamma_2)(\rho_{12} - \rho_{13})$$
$$- (\omega_a - i\gamma_2)(\rho_{12}^* - \rho_{13}^*)], \tag{11b}$$

$$\frac{\partial \langle \mu_y \rangle}{\partial t} = -\frac{E_x \mu_{sp}^2}{3\hbar}(\rho_{22} - \rho_{33}) + \frac{\mu_{sp}}{\sqrt{6}}[(\omega_a + i\gamma_2)(\rho_{12} + \rho_{13})$$
$$+ (\omega_a - i\gamma_2)(\rho_{12}^* + \rho_{13}^*)]. \tag{11c}$$

We end this section with two comments. First, as already pointed out, Eqs. (10) constitute a mean-field description of a system of atoms interacting with the EM field. In this approximation, a single atom interacts with other atoms through the electromagnetic field associated with their mean local density. Obviously, such an approach cannot account for specific atom-atom correlations, but it can describe collective effects in a system of atoms resulting from their interaction with the EM field.

Second, we note that this procedure can be easily generalized to yield the analogous three-dimensional coupled Maxwell-Liouville equations. To maintain spherical symmetry we would need to include an additional atomic level $|J = 1, M = 0\rangle$, which is coupled to the ground atomic state by E_z [44]. Obviously, it is also possible to expand the atomic basis and consider an additional excited manifold starting with $|J = 2, M\rangle$. Although the number of equations similar to Eqs. (10) grows significantly, modern analytical computer packages such as Mathematica [49] can easily handle the necessary algebra and subsequent computer coding. For a molecule without rotational symmetry, an average over the

angular distribution in the calculation of $\vec{P}$ from Eq. (5) may be used when relevant.

III. NUMERICAL APPROACH

To solve the system (1), (10), (11) of the coupled Maxwell-Liouville equations, we employ a generalized FDTD technique [50]. Within the FDTD, both the electric $\vec{E}$ and magnetic $\vec{H}$ fields are propagated in time and space by directly discretizing Maxwell's equations (1). This approach has several attractive technical features, including its numerical stability and the explicit description of the magnetic field. The latter is especially important if one considers structures with sharp corners, at which the tangential components of $\vec{H}$ have singularities. For our purpose, the main advantage of the FDTD approach is that the boundary conditions (i.e., the continuity of the tangential $\vec{H}$ and $\vec{E}$ components) are automatically maintained at all grid points owing to the use of the Yee cell [51]. This allows straightforward programming of the complex geometries.

For simulations of open systems, one needs to impose artificial absorbing boundaries in order to avoid numerical reflection of outgoing EM waves back to the simulation domain. Among the various approaches that address this numerical issue, the perfectly matched layers (PML) technique is considered to be the most powerful [52]. It reduces the reflection coefficient of outgoing waves at the simulation region boundary to $\sim 10^{-8}$. In essence, the PML approach surrounds the simulation domain by thin layers of nonphysical material that efficiently absorbs outgoing waves incident at any angle. We have implemented the most efficient and least memory variant of the method; the convolutional perfectly matched layers (CPML) absorbing boundaries [53]. Through extensive numerical experimentation, we have empirically determined the optimal parameters for the CPML boundaries that lead to almost no reflection of the outgoing EM waves at all incident angles.

In the calculations reported below we consider structures with a characteristic size much smaller than the incident wavelength. Hence it is a good approximation to excite such systems using a plane wave. The latter is accomplished via implementation of the total-field–scattered-field approach [50] within the FDTD.

We partition the FDTD scheme onto an array of parallel grid slices by dividing the cubic simulation cell into M xy slices, where M is the number of available processors. Point-to-point message passing interface (MPI) communication subroutines [54] are implemented at the boundaries between slices. The number of xy planes in each slice usually varies in the range from 15 to 20. All simulations are performed on the home-built 128-core AMD Opteron-based cluster at Arizona State University [55].

The numerical implementation of the proposed scheme is as follows:

(1) In the spatial regions occupied by atoms, the Maxwell equations are solved utilizing the standard FDTD algorithm. First, the magnetic field is updated according to Faraday's law, Eq. (1a). Next, using Ampère's law, Eq. (1b), we update the electric field with the macroscopic polarization current density

Eqs. (11), which is calculated using the density matrix of the previous time step. The EM fields in the regions occupied by metal are updated according to the auxiliary differential equation method [50], Eq. (3).

(2) With knowledge of local electric field components (stored in memory at two previous time steps) we update the density matrix at each spatial point on the grid according to Eqs. (10) using the fourth-order Runge-Kutta scheme [56].

(3) Finally, with knowledge of the electric field components and the updated density matrix we calculate the macroscopic polarization current $\frac{\partial \vec{P}}{\partial t}$ at each grid point according to (11). We have verified this scheme using several test cases. A most important test of numerical stability is to check that the condition $\mathrm{Tr}(\hat{\rho}) = 1$ is maintained at each time step. In all simulations this condition was perfectly satisfied with almost no dependence on incident field amplitude or other physical parameters. Another interesting test was to demonstrate the absence of self-interactions in our calculation. Such interactions often appear spuriously in mean-field calculations, whereupon a particle interacts with its own contribution to the mean density. In the present situation, however, the field produced by the oscillating dipole of a given atom propagates away from this atom and can affect it only through the polarization induced in other atoms or (in different setups) through reflection from the boundaries; both physically valid phenomena. We have verified that direct self-interaction is indeed absent in our calculation by solving Eqs. (1) and (10) for the case where the system occupies a single grid point. The same solution is obtained whether or not the polarization source term is included in Eq. (1b). Finally, we have compared our results and execution time of the proposed integration scheme with those obtained by Ziolkowski *et al.* [43]. We have implemented the numerical approach based on the predict-corrector method and atomic basis as used in [43] and compared it with ours (keeping in mind that μ_{sp} has to be renormalized by the factor of $\sqrt{3}$). The simulation data obtained using both approaches were in excellent agreement. However, execution times for the codes employing our approach were noticeably smaller.

With the solution of Eqs. (1), (10), and (11) obtained in this way, the following observables can be calculated:

(1) The scattered radiation can be computed as the difference between the total and the incident EM fields. At any detection point [e.g., that depicted as a red diamond in Fig. 1(b)], we can calculate the Poynting vector components associated with the scattered EM field. This may be integrated over a spherical boundary surrounding the atomic system to yield the total scattered radiation. These calculations can be accomplished in a transient mode to give the time-dependent response to an incident EM pulse, or in a steady state mode that yields the long time steady state response to cw incident radiation of a given frequency, ω_{in}. In the latter case we need to propagate the Maxwell-Liouville equations under the incident cw radiation until steady state is reached.

(2) Generally, for a given incident frequency ω_{in}, the outgoing field may exhibit different frequencies ω_{out} (with amplitudes obtained by Fourier transforming the scattered signal), making it possible to obtain the outgoing steady state flux (Poynting vector) in a given direction at any ω_{out} for a

given incident frequency. Integrating the outgoing flux over ω_{out} and displaying the result as a function of ω_{in} yields the absorption spectrum of the atomic cluster.

(3) A much easier way to calculate the steady state absorption lineshape is by calculating the steady state relaxation flux of the excited state populations according to

$$-\frac{dE}{dt} \approx \hbar\omega_a\gamma_1 \int d^3r [\rho_{22}(\vec{r}) + \rho_{33}(\vec{r})], \qquad (12)$$

where the integral is taken over cluster volume [57]. Equation (12) expresses, for any given incoming frequency, the rate of energy dissipation by the molecular system, which at steady state should be equal to the rate of energy absorption at that frequency.

(4) For some applications the short-pulse method (SPM) [46] can save substantial computing effort. In this approach we use an ultrashort incident pulse with a wide bandwidth, which is almost flat in the spectral region of interest (in our simulations the incident pulse duration was set at 0.36 fs, which corresponds to a flat spectrum throughout the frequency domain considered in this paper). Such a pulse can be represented as a coherent linear superposition of cw plane waves with different ω_{in}. We then propagate the Maxwell-Liouville equations for several picoseconds (the total propagation time has to be significantly longer than the lifetime of the excited states of an atom, $1/\gamma_1$) and take the Fourier transform of the calculated field. Under conditions of linear response and elastic scattering (i.e., when $\omega_{\text{out}} = \omega_{\text{in}}$), the Fourier component at frequency ω contains all the information relevant to a cw process at frequency ω.

When applicable, the SPM can save substantially on computation time, since it yields the system response at many frequencies from one short-time computation. It is important to understand its shortcomings. Two limitations, mentioned above, are obvious: this method is applicable only for a linear response and only when the light scattering process is elastic. Both limitations are associated with the requirement that a given incident frequency can give rise to a response only at the same frequency. A third limitation is important in the present context, because Eqs. (10c) and (10d) are inherently nonlinear. Linearity is obtained when ρ_{22} and ρ_{33} may be neglected and ρ_{11} taken as constant in these equations. In this case, the steady state solutions for ρ_{12} and ρ_{13} and, therefore, the polarization Eq. (5) oscillate with the incident frequency, as required. Care has to be exercised if one attempts to calculate the steady state excitation, $\rho_{22} + \rho_{33}$, in this method. An approximation may be obtained if the incident frequency is close to the atomic transition frequency ω_a by taking the Fourier transform at $\omega = 0$ (i.e., the time average) of the resulting time-dependent signal.

The method, as described, cannot describe spontaneous emission (i.e., fluorescence) since the latter is a quantum effect associated with the quantum nature of the radiation field. It has been demonstrated [58] that the effect of spontaneous emission can be partially accounted for by imposing a classical stochastic field on the system. Obviously, classical EM noise cannot mimic vacuum fluctuations; in particular, it can induce excitation of ground-state molecules while vacuum fluctuations can lead only to radiative damping of excited molecules. One can use this trick to study time evolution in

a system which is initially inverted; that is, all molecules are in the excited state. In this case, the induction of emission by the EM noise will soon lead to a dominant signal of induced emission that does not depend much on the nature of that noise, provided the latter is weak enough. This method has been successfully used to simulate superradiance [58,59] and gain [60] within the FDTD approach. However, this method cannot be used to generate fluorescence in a system of mostly ground-state molecules ($\rho_{22} + \rho_{33} \ll \rho_{11}$), where the main effect of such noise will be to induce unphysical molecular excitation.

IV. RESULTS AND DISCUSSION

The simulation setup is shown in Fig. 1(b): an atomic cluster is excited with an x-polarized low-intensity plane wave propagating in the y direction. We use low-intensity incoming fields (our incident electric field was fixed at 1 V/m) in order to ensure linearity of the system response [61]. Equations (1), (10), and (11) are then evolved to yield the electric and magnetic fields as functions of time and position. In the current studies we focus on the y component of the Poynting vector, $S_y \sim E_x H_z$, as the observable of interest.

Figure 2 presents a direct comparison of two methods: the SPM approach and the cw scheme. The scattering signals obtained from the two methods are in excellent agreement. Also shown is the absorption spectrum from the cw calculation using Eq. (12). The absorption lineshape (normalized so that it matches the scattering signals at the peak) also leads to a nearly identical lineshape, except that it exhibits a more pronounced resonance near the atomic transition frequency.

It is not surprising, but still providing a consistency check, that at the very low densities ($n_a < 10^{24}$ m^{-3}) and zero dephasing, our simulations are in the perfect agreement with the Clausius-Mossotti approximation described below. Moreover, calculations in which the polarization current term
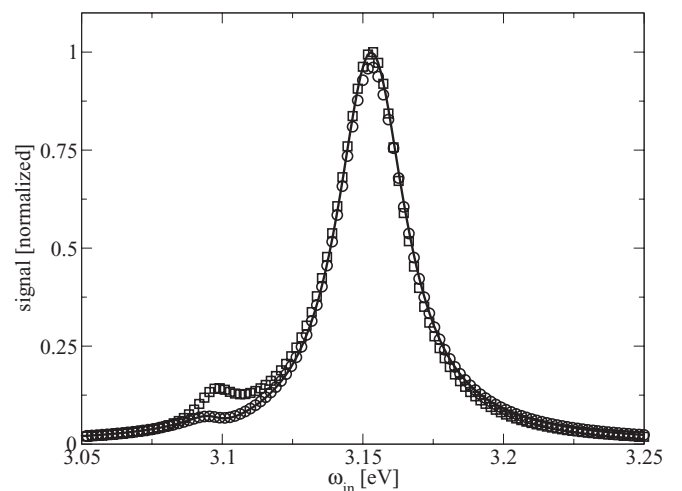

FIG. 2. Scattering intensity as a function of the incoming frequency ω_{in} calculated within the SPM approach (solid line) and cw scheme (circles). Normalized absorption [see Eq. (12)] is shown as squares. Simulations are performed for the cluster with the following parameters: $\omega_a = 3.1$ eV, $R = 25$ nm, $n_a = 7 \times 10^{25}$ m^{-3}, $\gamma_1 = 10^{12}$ s^{-1}, $\gamma_p = 10^{13}$ s^{-1}, $\mu_{sp} = 25$ Debye.
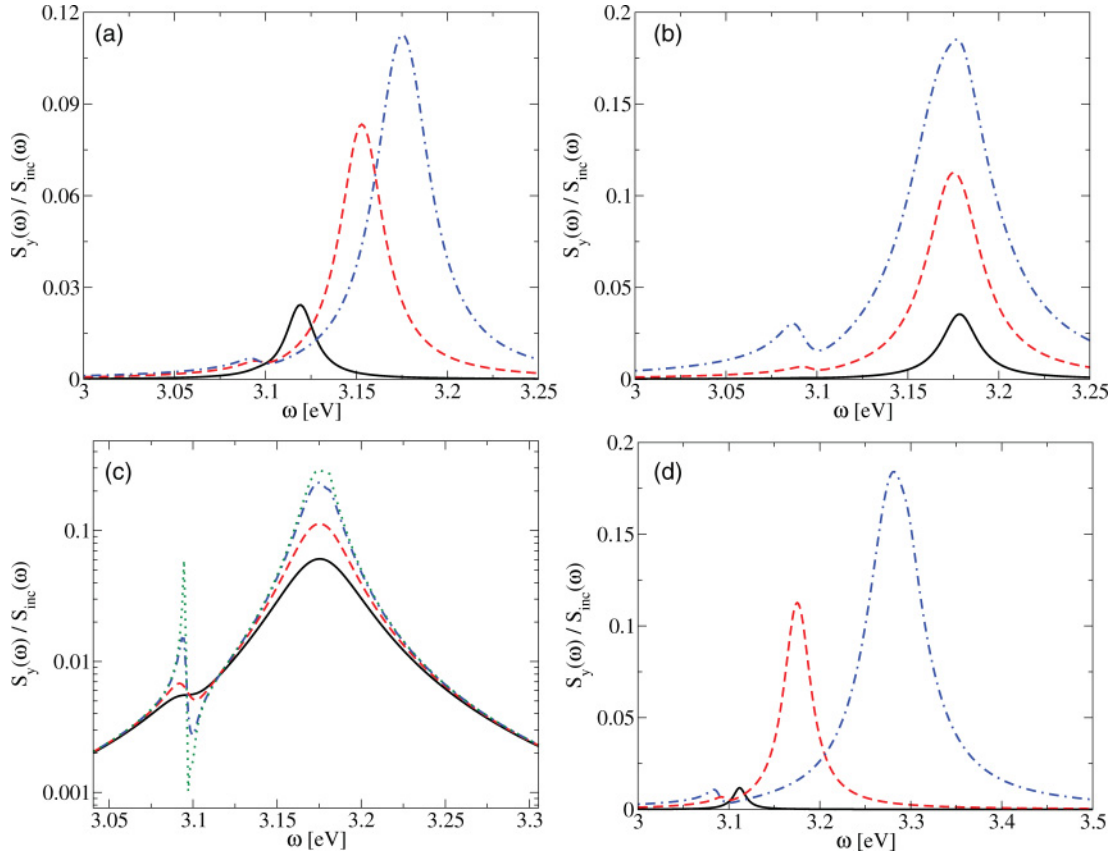
FIG. 3. (Color online) Linear optics of atomic clusters with $\omega_a = 3.1$ eV, $\gamma_1 = 10^{12}$ s^{-1}. Panel (a) shows the scattering intensity as a function of the incident frequency for three atomic densities, n_a. Black solid line: $n_a = 2.5 \times 10^{25}$ m^{-3} (ideal gas at atmospheric pressure and room temperature), red dashed line: $n_a = 7 \times 10^{25}$ m^{-3}, blue dash-dotted line: $n_a = 10^{26}$ m^{-3}. Other parameters are $R = 25$ nm, $\gamma_p = 10^{13}$ s^{-1}, and $\mu_{sp} = 25$ Debye. Panel (b) shows the same as in panel (a) for the radii R of three clusters. Black (solid), red (dashed), and blue (dash-dotted) lines show scattering intensity results for $R = 15$, 25, and 35 nm, respectively. Other parameters are $n_a = 10^{26}$ m^{-3}, $\gamma_p = 10^{13}$ s^{-1}, and $\mu_{sp} = 25$ Debye. Panel (c) shows the same as in panels (a) and (b) (now shown in logarithmic scale), but for four pure dephasing rates γ_p. Black (solid) line: $\gamma_p = 2 \times 10^{13}$ s^{-1}, red (dashed) line: $\gamma_p = 10^{13}$ s^{-1}, blue (dash-dotted) line $\gamma_p = 2 \times 10^{12}$ s^{-1}, green (dotted) line shows the data without pure dephasing $\gamma_p = 0$ s^{-1}. Other parameters are $R = 25$ nm, $n_a = 10^{26}$ m^{-3}, and $\mu_{sp} = 25$ Debye. Panel (d) shows the same as in panels (a)–(c), but for three values of the matrix element of the dipole moment μ_{sp}. Black (solid), red (dashed), and blue (dash-dotted) lines correspond to atomic systems characterized by $\mu_{sp} = 10$, $\mu_{sp} = 25$, and $\mu_{sp} = 40$ Debye, respectively. Other parameters are $R = 25$ nm, $n_a = 10^{26}$ m^{-3}, $\gamma_1 = 10^{12}$ s^{-1}, and $\gamma_p = 10^{13}$ s^{-1}.

in (1b) was neglected (i.e., the atoms are not coupled to each other through their mutual interaction with the radiation field but rather are driven only by external incident radiation), were in perfect agreement with the data produced by the full self-consistent computations in the limit of low densities.

Figure 3 summarizes the main results of our SPM calculations (note that we performed a direct comparison of the SPM data with that obtained via the cw scheme for every set of parameters discussed below). First, the dependence of the scattering intensity on the density of atoms in the cluster is depicted in Fig. 3(a). The atomic transition frequency is fixed at $\omega_a = 3.1$ eV (see figure caption for the rest of the simulation parameters). The scattering radiation clearly exhibits two resonances: The first is a relatively weak response close to (slightly below) the atomic transition frequency. The second is a strong and broad peak at a higher frequency that moves to the blue at larger atomic densities. Additional simulations presented in Fig. 4 show that the intensity of the high-frequency mode (unlike the low-frequency mode) scales as n_a^2 for the low

density of atoms, suggesting a possible collective nature of the peak. It should be noted that this collective mode is noticeably wider than the atomic transition resonance.

The dependence of the scattering intensity on the cluster's size is shown in Fig. 3(b). The low-energy resonance exhibits a redshift, when a radius of the cluster increases, while the resonant frequency of the high-energy mode does not change with cluster size. However, it becomes significantly wider for larger clusters, which has been observed experimentally [62].

One of the advantages of the present calculations over the standard approach based on a dielectric model is the ability to examine the influence of the dephasing rate on optical properties. Figure 3(c) shows simulation results obtained at three pure dephasing rates γ_p, including the case without pure dephasing. We should note that, at small γ_p numerical simulations tend to become hard to converge at frequencies near the collective resonance (in our case this occurs for $\gamma_p < 4 \times 10^{12}$ s^{-1}). While for relatively high dephasing rates regular simulations require spatial steps δx on the order of
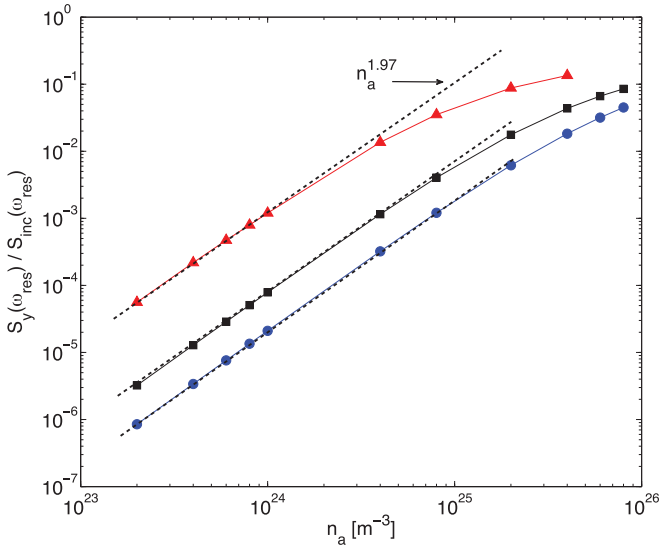
FIG. 4. (Color online) Scattering intensity (shown in double logarithmic scale) at the high-frequency resonance, ω_{res}, as a function of the atomic density n_a for three pure dephasing rates γ_p Blue circles: $\gamma_p = 2 \times 10^{13}$ s^{-1}, black rectangles: $\gamma_p = 10^{13}$ s^{-1}, red triangles: $\gamma_p = 2 \times 10^{12}$ s^{-1}. Other parameters are $\omega_a = 3.1$ eV, $\gamma_1 = 10^{12}$ s^{-1}, $R = 25$ nm, $n_a = 10^{26}$ m^{-3}, and $\mu_{sp} = 25$ Debye. The straight dashed lines represent fitting for each set of data, demonstrating nearly ideal quadratic dependence on n_a at low densities.

1 nm, the case without pure dephasing should be explored at $\delta x < 0.2$ nm. It is interesting to note that the collective mode, while decreasing its width with the decrease of the dephasing rate, is still significantly wider than the atomic transition peak. In contrast, the low-frequency peak becomes narrower with decreasing dephasing rate, with its width approaching γ_1. Note that the scattering actually shows a dip at the atomic frequency, with the low-frequency peak slightly below it.

Figure 3(d) explores how the scattering is affected by the matrix element of the atomic dipole moment μ_{sp}. Not surprisingly, the result for increasing μ_{sp} is qualitatively similar to that obtained with increasing atomic density. It is seen that larger μ_{sp} results in a blueshift of the higher-frequency collective mode and in a redshift of the lower-frequency mode. The former shows a quadratic dependence of the resonant frequency on the dipole moment, which has been theoretically discussed for the case of a sphere with uniformly distributed linear quantum dipoles [63].

It is useful, for the sake of comparison, to consider the simplest theoretical description for the optical response of our system, by modeling it as a dielectric particle with a dielectric response function taken from the Clausius-Mossotti expression

$$\varepsilon = \frac{1 + 2x}{1 - x}, \tag{13}$$

where $x \equiv \frac{4\pi}{3} n\alpha$, n is the number density of atoms, and α is the atomic polarizability. The absorption lineshape can be calculated [64] as the ratio between the dissipated power, $P_{\text{diss}} = \frac{1}{2} \int d^3 r \sigma |E|^2$ and the incident flux, $J_{\text{in}} = c|E_{\text{in}}|^2/(8\pi)$, where $\sigma = \frac{\omega_{\text{in}}}{4\pi} \text{Im}(\varepsilon)$ is the conductivity, ε is the dielectric response function, E is the electric field in the particle, E_{in} is the incident

electric field, and c is the speed of light. For a small spherical particle [65],

$$E = \frac{3}{\varepsilon + 2} E_{\text{in}}. \tag{14}$$

Using these expressions we obtain the absorption cross-section of a small spherical particle of volume Ω in the form

$$\sigma_a = \frac{P_{\text{diss}}}{J_{\text{in}}} = \Omega \frac{\omega_{\text{in}}}{c} \left| \frac{3}{\varepsilon + 2} \right|^2 \text{Im}(\varepsilon) = \frac{16\pi}{3} n \Omega \, \text{Im}(\alpha). \tag{15}$$

The imaginary part of the molecular optical polarizability is essentially a Lorentzian resonance peaked at the atomic transition frequency ω_a. We see that the absorption cross section in the Clausius-Mossotti approximation is proportional to the number of particles and to the absorption of a single particle, as would be predicted for a system of noninteracting particles. On the same level of theory, the dipole induced on the particle is [65]

$$\vec{\mu} = \frac{\varepsilon - 1}{\varepsilon + 2} \frac{3\Omega}{4\pi} \vec{E}_{\text{in}} = n\Omega \alpha \vec{E}_{\text{in}}, \tag{16}$$

and, since the scattered light is proportional to $|\mu|^2$, it is predicted to go like the square of the number of particles and to have a similar resonant behavior as a function of the incident frequency. Equations (15) and (16) describe essentially a system of noninteracting particles occupying a volume with linear dimensions much smaller than the radiation wavelength that respond coherently to the incident radiation. This approximation is valid at low atomic density. We will see below how dephasing and through-field interatomic interactions at higher densities affect this behavior.

While the calculation procedure applied here provides a route to explore the effect of dephasing on the optical response of atomic and molecular clusters, further studies will be needed in order to determine how much of this effect was indeed captured in our simulations. The destruction of phase is affected within our calculations on the mean-field evolution of a single atom, feeling the effects of others through their mutual interaction with the radiation field. It is not obvious that this mean-field implementation can capture the full physics of atoms going out of phase from each other. We leave this important technical question to a future study.

It is informative to explore the spatial dependence of EM intensity, $I \sim E_x^2 + E_y^2$, at resonant conditions. Figure 5 shows intensity distributions calculated using steady state solutions of Maxwell-Liouville equations for the two resonance modes. Clearly the EM intensity at the lower resonant frequency is mainly localized on the surface of the cluster exhibiting a dipole radiation pattern similar to the EM intensity distributions seen at the plasmon resonance for a single metal nanoparticle [13]. The collective high-frequency mode is distributed over the entire volume of the particle, where all atoms coherently participate in the radiation process. This suggests that the high-frequency mode is more collective in nature than the low-frequency one, consistent with its large density-dependent shift from the atomic frequency and its n_a^2 scaling at low densities. The low-frequency mode, involving fewer surface atoms, may be more atomic in nature.

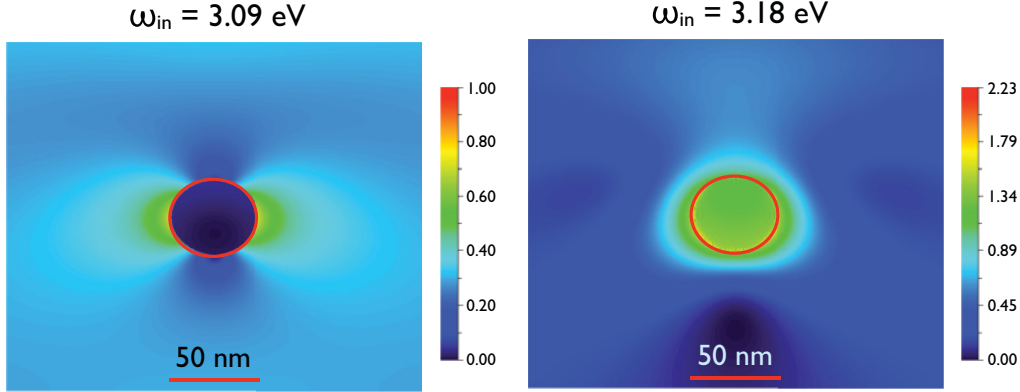ω_{in} = 3.09 eV

ω_{in} = 3.18 eV

FIG. 5. (Color online) Spatial distributions of EM intensity (normalized to the incident intensity) in logarithmic scale at the low-frequency resonance (left panel) and the high-frequency resonance (right panel). Cluster's parameters are $\omega_a = 3.1$ eV, $\gamma_1 = 10^{12}$ s^{-1}, $\gamma_p = 10^{13}$ s^{-1}, $R = 25$ nm, $n_a = 10^{26}$ m^{-3}, and $\mu_{sp} = 25$ Debye.

It is important to note, however, that this is not a single-atom response since it clearly shifts with increasing atomic density.

Optical properties of molecular aggregates resonantly coupled to plasmonic materials have been a subject of extensive research for the past several years. Sugawara *et al.* [66] demonstrated significant modification of transmission and reflection spectra of a gold film with deposited J aggregates. It has been shown experimentally that SPP resonances notably affect molecular electronic structure leading to resonance splitting [33]. The latter was proposed to be used for controlling optics of such hybrid material using femtosecond laser pulses [67]. Moreover, core-shell metal NPs with a shell comprised of optically active molecules have been recently

studied experimentally [68]. To demonstrate the generality of our approach we present simulations of the core-shell particle schematically depicted in the inset of Fig. 6. Here, a silver nanoparticle is shelled by a resonant atomic layer, with atomic transition frequency equal to the SPP resonance of silver, $\omega_a = 3.61$ eV. The optical properties of silver are described within the Drude model with parameters as in [18]. The hollow atomic shell exhibits a doubled collective mode (red dashed line in Fig. 6), which corresponds to the symmetry of the problem and can be understood within the plasmon hybridization model proposed for noble-metal core-shell particles [69]. The important observation is a clear splitting of the SPP mode with an additional strong peak centered near the atomic transition frequency (blue dash-dotted line in Fig. 6). The observed splitting as indicated in [33] is due to the strong optical coupling of atoms with the SPP mode.
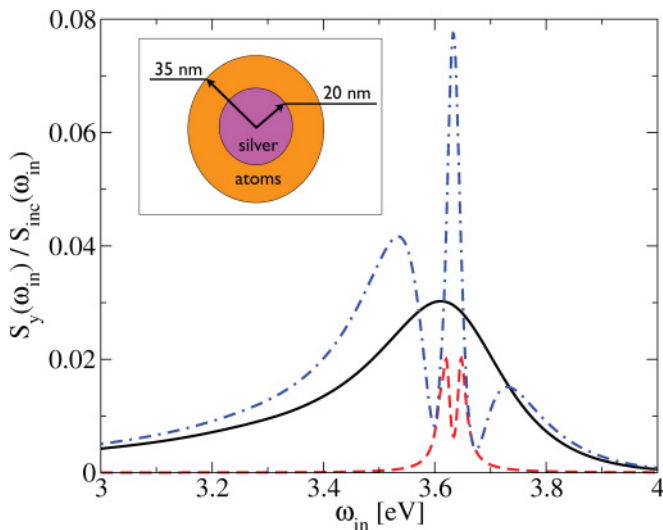

FIG. 6. (Color online) Scattering intensity as a function of the incident frequency for the core-shell particle shown in the inset. Black solid line shows the data for the silver nanoparticle without atomic shell, red dashed line presents simulations for the hollow atomic shell, and blue dash-dotted line demonstrates results obtained for atomic shell with a silver core. Parameters of the simulations are $n_a = 2.5 \times 10^{25}$ m^{-3}, $\omega_a = 3.61$ eV, $\gamma_1 = 10^{12}$ s^{-1}, $\gamma_p = 10^{13}$ s^{-1}, and $\mu_{sp} = 25$ Debye.

V. CONCLUSION

We have presented a self-consistent electrodynamical model based on coupled Maxwell-Liouville equations that takes into account arbitrary polarization of the incident field. The proposed model is applied to investigate the linear optical response of nanoscale atomic clusters in two dimensions, merging classical electrodynamics with a quantum mechanical description of atoms. The calculations can capture collective effects that play pivotal roles in the electrodynamics of nanosystems and, within the limitations discussed below, include the effect of dephasing on the optical response of these systems.

We have found that spherical atomic clusters exhibit two well-distinguished resonances. The low-energy resonance is close to the atomic transition frequency of individual atoms. The EM intensity distribution at this resonance is localized near the surface of a cluster. The high-energy mode, where all atoms in the cluster coherently participate in the scattering, has a clear collective nature. The dependence of the scattering intensity on various parameters was considered. It was demonstrated that pure dephasing plays an important role in the scattering and absorption. Moreover,

we successfully applied our formalism to more complex systems, which comprise a resonant atomic shell and a silver core.

Applications of the proposed scheme are many and vast. They range from complete three-dimensional descriptions of nanoparticles resonantly coupled to ensembles of quantum particles to nonlinear optical phenomena at the nanoscale. We note that our scheme can be extended to molecular systems, where one may investigate Raman processes. At the same time, we have indicated physically significant open technical issues. One is the limited ability of an approach based on classical electrodynamics to describe spontaneous emission and hence fluorescence. To account for such phenomena we need to modify the Maxwell-Liouville equations (1), (10), and (11), so as to take into account the quantum nature of the radiation field, possibly using the quantization schemes described in Refs. [70–72] or [73,74] (which were shown to be equivalent [75]). Another is the need to examine the adequacy of mean-field calculations of dephasing. All these will be subjects of our continuing studies.

ACKNOWLEDGMENTS

[1] M. Li, W. H. P. Pernice, C. Xiong, T. Baehr-Jones, M. Hochberg, and H. X. Tang, Nature (London) **456**, 480 (2008).

[2] T. W. Ebbesen, C. Genet, and S. I. Bozhevolnyi, Phys. Today **61**, 44 (2008).

[3] R. F. Oulton, V. J. Sorger, T. Zentgraf, R.-M. Ma, C. Gladden, L. Dai, G. Bartal, and X. Zhang, Nature (London) **461**, 629 (2009).

[4] S. Chu, Science **253**, 861 (1991).

[5] J. Homola, Anal. Bioanal. Chem. **377**, 528 (2003).

[6] I. H. El-Sayed, X. Huang, and M. A. El-Sayed, Nano Lett. **5**, 829 (2005).

[7] I. Romero, J. Aizpurua, G. W. Bryant, and F. J. Garcia de Abajo, Opt. Express **14**, 9988 (2006).

[8] J. Zhang, Y. Fu, M. H. Chowdhury, and J. G. Lakowicz, Nano Lett. **7**, 2101 (2007).

[9] H. Szmacinski, J. R. Lakowicz, J. M. Catchmark, K. Eid, J. P. Anderson, and L. Middendorf, Appl. Spectrosc. **62**, 733 (2008).

[10] Y. N. Xia, W. Y. Li, P. H. C. Camargo, and X. M. Lu, Nano Lett. **9**, 485 (2009).

[11] K. L. Wustholz, A.-I. Henry, J. M. McMahon, R. G. Freeman, N. Valley, M. E. Piotti, M. J. Natan, G. C. Schatz, and R. P. Van Duyne, J. Am. Chem. Soc. **132**, 10903 (2010).

[12] M. Rycenga, P. H. C. Camargo, W. Li, C. H. Moran, and Y. Xia, J. Phys. Chem. Lett. **1**, 696 (2010).

[13] W. A. Murray and W. L. Barnes, Adv. Mater. **19**, 3771 (2007).

[14] K. L. Kelly, E. Coronado, L. L. Zhao, and G. C. Schatz, J. Phys. Chem. B **107**, 668 (2003).

[15] M. Sukharev, P. R. Sievert, T. Seideman, and J. B. Ketterson, J. Chem. Phys. **131**, 034708 (2009).

[16] S. A. Maier, M. L. Brongersma, P. G. Kik, S. Meltzer, A. A. G. Requicha, and H. A. Atwater, Adv. Mater. **13**, 1501 (2001).

[17] E. Le Ru and P. G. Etchegoin, *Principles of Surface-Enhanced Raman Spectroscopy and Related Plasmonic Effects* (Elsevier, San Diego, 2008).

[18] M. Sukharev and T. Seideman, J. Phys. Chem. A **113**, 7508 (2009).

[19] Y. Fedutik, V. V. Temnov, O. Schops, U. Woggon, and M. V. Artemyev, Phys. Rev. Lett. **99**, 136802 (2007).

[20] X. Xu, B. Sun, P. R. Berman, D. G. Steel, A. S. Bracker, D. Gammon, and L. J. Sham, Science **317**, 929 (2007).

[21] V. K. Komarala, A. L. Bradley, Y. P. Rakovich, S. J. Byrne, Y. K. Gunko, and A. L. Rogach, Appl. Phys. Lett. **93**, 123102 (2008).

[22] A. A. Toropov, T. V. Shubina, V. N. Jmerik, S. V. Ivanov, Y. Ogawa, and F. Minami, Phys. Rev. Lett. **103**, 037403 (2009).

[23] D. E. Gomez, K. C. Vernon, P. Mulvaney, and T. J. Davis, Nano Lett. **10**, 274 (2010).

[24] X.-R. Su, W. Zhang, L. Zhou, X.-N. Peng, and Q.-Q. Wang, Opt. Express **7**, 6516 (2010).

[25] M. Achermann, J. Phys. Chem. Lett. **1**, 2837 (2010).

[26] M. L. Andersen, S. Stobbe, A. S. Sorensen, and P. Lodahl, Nat. Phys. **7**, 215 (2010).

[27] D. Ratchford, F. Shafiei, S. Kim, S. K. Gray, and X. Li, Nano Lett. **11**, 1049 (2011).

[28] E. Dulkeith, A. C. Morteani, T. Niedereichholz, T. A. Klar, J. Feldmann, S. A. Levi, F. C. J. M. van Veggel, D. N. Reinhoudt, M. Moller, and D. I. Gittins, Phys. Rev. Lett. **89**, 203002 (2002).

[29] C. Bonnand, J. Bellessa, and J. C. Plenet, Phys. Rev. B **73**, 245330 (2006).

[30] S. Pan, Z. Wang, and L. J. Rothberg, J. Phys. Chem. B **110**, 17383 (2006).

[31] T. Uwada, R. Toyota, H. Masuhara, and T. Asahi, J. Phys. Chem. C **111**, 1549 (2007).

[32] W. Ni, Z. Yang, H. Chen, L. Li, and J. Wang, J. Am. Chem. Soc. **130**, 6692 (2008).

[33] A. Salomon, C. Genet, and T. W. Ebbesen, Angew. Chem. **121**, 8904 (2009).

[34] N. I. Cade, T. Ritman-Meer, and D. Richards, Phys. Rev. B **79**, 241404 (2009).

[35] S. Hayashi, A. Maekawa, S. C. Kim, and M. Fujii, Phys. Rev. B **82**, 035441 (2010).

[36] T. Sen, S. Jana, S. Koner, and A. Patra, J. Phys. Chem. C **114**, 707 (2010).

[37] C. Garcia-Segundo, H. Yan, and M. S. Zhan, Phys. Rev. A **75**, 030902 (2007).

[38] E. Vetsch, D. Reitz, G. Sague, R. Schmidt, S. T. Dawkins, and A. Rauschenbeutel, Phys. Rev. Lett. **104**, 203603 (2010).

[39] P. Xu, X. He, J. Wang, and M. Zhan, Opt. Lett. **35**, 2164 (2010).

[40] F. Le Kien and K. Hakuta, Phys. Rev. A **81**, 063808 (2010).

[41] Y. Sun and Y. Xia, Science **298**, 2176 (2002).

[42] R. W. Ziolkowski, J. M. Arnold, and D. M. Gogny, Phys. Rev. A **52**, 3082 (1995).

[43] G. Slavcheva, J. M. Arnold, I. Wallace, and R. W. Ziolkowski, Phys. Rev. A **66**, 063418 (2002).

[44] A. Fratalocchi, C. Conti, and G. Ruocco, Phys. Rev. A **78**, 013806 (2008).

[45] K. Lopata and D. Neuhauser, J. Chem. Phys. **131**, 014701 (2009).

[46] S. K. Gray and T. Kupka, Phys. Rev. B **68**, 045415 (2003).

[47] Note that, as in many studies of this type, a two-dimensional solution does not correspond to a two-dimensional system but to the three-dimensional system of infinite extent in the z direction, obtained by displacing the xy cross section along the z axis. The densities defined above remain per-unit-volume quantities.

[48] H.-P. Breuer and F. Petruccione, *The Theory of Open Quantum Systems* (Oxford University Press, New York, 2002).

[49] [http://budker.berkeley.edu/ADM/index.html].

[50] A. Taflove and S. C. Hagness, *Computational Electrodynamics: The Finite-Difference Time-Domain Method*, 3rd ed. (Artech House, Boston, 2005).

[51] K. S. Yee, IEEE Trans. Antennas Propag. **14**, 302 (1966).

[52] J.-P. Berenger, in *Synthesis Lectures on Computational Electromagnetics #8* (Morgan & Claypool Publishers, San Rafael, California, 2007).

[53] J. A. Roden and S. D. Gedney, Microw. Opt. Techn. Let. **27**, 334 (2000).

[54] P. S. Pacheco, *Parallel Programming with MPI* (Morgan Kaufmann Publishers, San Francisco, California, 1997).

[55] [http://plasmon.poly.asu.edu].

[56] E. Hairer, S. P. Nørsett, and G. Wanner, *Solving Ordinary Differential Equations* 2nd rev. edn., (Springer-Verlag, Berln, New York, 1993) Springer Series in Computational Mathematics, 8, 14.

[57] In the actual calculations, ρ_{22} and ρ_{33} exhibit small low-frequency oscillations that we eliminate by time averaging.

[58] J. Andreasen and H. Cao, J. Lightwave Technol. **27**, 4530 (2009).

[59] Y. Huang, Z. Zhang, and S. Ho, in *Frontiers in Optics*, *OSA Technical Digest (CD), Optical Society of America, 2008*, paper FThP5.

[60] J. Andreasen and H. Cao, Phys. Rev. A **82**, 063835 (2010).

[61] We have numerically verified that all results of our simulations scale linearly with the incident intensity.

[62] K. Misawaa, H. Yaob, T. Hayashib, and T. Kobayashi, Chem. Phys. Lett. **183**, 113 (1991).

[63] S. Prasad and R. J. Glauber, Phys. Rev. A **82**, 063805 (2010).

[64] J. Gersten and A. Nitzan, J. Chem. Phys. **75**, 1139 (1981).

[65] J. D. Jackson, *Classical Electrodynamics* (John Wiley and Sons, New York, 1962).

[66] Y. Sugawara, T. A. Kelf, J. J. Baumberg, M. E. Abdelsalam, and P. N. Bartlett, Phys. Rev. Lett. **97**, 266808 (2006).

[67] P. Vasa, R. Pomraenke, G. Cirmi, E. De Re, W. Wang, S. Schwieger, D. Leipold, E. Runge, G. Cerullo, and C. Lienau, ACS Nano **12**, 7559 (2010).

[68] D. D. Lekeufack, A. Brioude, A. W. Coleman, P. Miele, J. Bellessa, L. D. Zeng, and P. Stadelmann, Appl. Phys. Lett. **96**, 253107 (2010).

[69] E. Prodan and P. Nordlander, J. Chem. Phys. **120**, 5444 (2004).

[70] T. Gruner and D.-G. Welsch, Phys. Rev. A **53**, 1818 (1996).

[71] H. T. Dung, L. Knoll, and D.-G. Welsch, Phys. Rev. A **57**, 3931 (1998).

[72] S. Scheel, L. Knoll, and D.-G. Welsch, Phys. Rev. A **58**, 700 (1998).

[73] A. Tip, Phys. Rev. A **57**, 4818 (1998).

[74] A. Tip, Phys. Rev. A **69**, 013804 (2004).

[75] A. Tip, L. Knoll, S. Scheel, and D.-G. Welsch, Phys. Rev. A **63**, 043806 (2001).